

## Symmetry-based imaging condition in time reversed acoustics

T. J. Ulrich, M. Griffa, and B. E. Anderson

Citation: [Journal of Applied Physics](#) **104**, 064912 (2008); doi: 10.1063/1.2980323

View online: <http://dx.doi.org/10.1063/1.2980323>

View Table of Contents: <http://scitation.aip.org/content/aip/journal/jap/104/6?ver=pdfcov>

Published by the [AIP Publishing](#)

---

### Articles you may be interested in

[Acoustic emission localization in complex dissipative anisotropic structures using a one-channel reciprocal time reversal method](#)

J. Acoust. Soc. Am. **130**, 168 (2011); 10.1121/1.3598458

[Active waveguide Green's function estimation with application to time-reversal focusing without a probe source in a range-independent waveguide](#)

J. Acoust. Soc. Am. **120**, 2755 (2006); 10.1121/1.2355538

[Time-reversal-based imaging and inverse scattering of multiply scattering point targets](#)

J. Acoust. Soc. Am. **118**, 3129 (2005); 10.1121/1.2042987

[A method of images for a penetrable acoustic waveguide](#)

J. Acoust. Soc. Am. **113**, 194 (2003); 10.1121/1.1523082

[Time reversed acoustics](#)


AIP Conf. Proc. **557**, 3 (2001); 10.1063/1.1373736

---



**AIP** | Journal of Applied Physics

Meet The New Deputy Editors

|   |                           |   |                      |   |                       |
|---|---------------------------|---|----------------------|---|-----------------------|
|  | <b>Christian Brosseau</b> |  | <b>Laurie McNeil</b> |  | <b>Simon Phillpot</b> |
|---|---------------------------|---|----------------------|---|-----------------------|

# Symmetry-based imaging condition in time reversed acoustics

T. J. Ulrich,<sup>a)</sup> M. Griffa,<sup>b)</sup> and B. E. Anderson

*EES-11, Los Alamos National Laboratory, Los Alamos, New Mexico, 87545, USA*

(Received 23 May 2008; accepted 20 July 2008; published online 25 September 2008)

Introduced in this paper is a new method of determining and investigating focal positions of time reversed elastic wave fields. This method exploits the temporally symmetric nature of time reversed acoustics focused signals as they are akin to the autocorrelation function of the forward propagation received signals. Contrasting this symmetry with the degree of asymmetry at regions away from the focal location provides details about the original source that cannot be retrieved when using other standard imaging conditions. © 2008 American Institute of Physics. [DOI: 10.1063/1.2980323]

## I. INTRODUCTION

Time reversed acoustics (TRA) is a method used to focus mechanical wave energy onto a specific location at a specific time. Basically, for a linear lossless medium, it relies upon the covariance of the elastodynamics wave equation under the transformation  $t \rightarrow -t$  (time inversion) and the spatial reciprocity principle.<sup>1-3</sup> A typical TRA experiment employs a set of transducers, called a time reversal mirror (TRM),<sup>4,5</sup> which detect forward propagation signals produced by an active source(s) and eventually by a scatterer(s) [passive source(s)] inside the medium of propagation (linear scatterers such as inhomogeneities, voids, boundaries, and/or nonlinear scatterers such as microcracks, grain boundaries, and contact interfaces). These signals are digitalized, reversed in time, and broadcast from the same transducers, now acting as sources. The time reversed (TR) backpropagated waves retrace the forward propagation paths and focus onto the original source(s) location(s), like in a movie played backward.<sup>3,6,7</sup>

The retrofocusing on active sources and scatterers occurs also in weakly attenuative media (invariant in time). In fact, it has been shown that the previously described process, also known as the time reversal process (TRP),<sup>8</sup> is equivalent to a matched filtering<sup>8-10</sup> in space and time. A filter matched to a signal maximizes the signal-to-noise ratio of that signal.<sup>11,12</sup> In the case of the TRP, the input signal to the matched filter is the original forward propagation source signal, the output is the time reversal backpropagation signal and the maximization corresponds to enhancing the output at the exact time of retrofocus at the original source location.<sup>8</sup>

It follows that TRA can be used to localize sources and to reconstruct source signals, the reconstruction quality depending upon the number of elements of the TRM and the attenuation properties of the medium, among others. Specific signal processing enhancement methods, based upon TRA, have been developed for the selective localization of multiple (pointlike or extended) sources and scatterers in complex heterogeneous media,<sup>13-20</sup> including nonlinear scatterers.<sup>21-24</sup>

Once a TR focus is created in space and time, the wave energy continues to propagate back outward away from the focal location. Thus TRA is not based on a complete reversal of time of the forward propagation, due not only to the attenuation in the medium but also to the lack of an energy sink at the source location.<sup>2,25</sup> Essentially, energy coalescing to form a focus propagates inward toward the focal location and then propagates back outward away from the focal location.<sup>2</sup> Thus, the TRP is temporally symmetric as evinced by its mathematical description, based on the autocorrelation of signals and their properties.<sup>8,26</sup> Heuristically, from a signal processing point of view, the TRP can be represented in the following way. The forward propagation source signal at one location  $\mathcal{A}$  in the medium is convolved with the Green function from position  $\mathcal{A}$  to position  $\mathcal{B}$ , the latter being the TRM location (we consider for simplicity a single element TRM). The resulting signal is then TR and convolved with the Green function from  $\mathcal{B}$  to  $\mathcal{A}$  (identical to the Green function from  $\mathcal{A}$  to  $\mathcal{B}$  if the spatial reciprocity principle holds) to give the reconstructed signal at the original source position. This process is not completely identical to an autocorrelation signal. In fact, the reconstructed source signal is then defined as the convolution-in-time between the autocorrelation function of the Green function from  $\mathcal{A}$  to  $\mathcal{B}$  and the TR version of the original source signal, whereas a true autocorrelation signal is simply the convolution in time of the signal with its TR version. However, both the demonstration of the equivalence between the TRP and a matched filtering<sup>8,9</sup> and our recent study of the robustness of the TRP in the reconstruction of source signals in solid media<sup>26</sup> confirm that in general the time reversal reconstructed source signal is temporally symmetric.

TRA focusing improves with an increasing number of employed transducers in a TRM. However, TRA becomes more practical and exploitable (e.g., for nondestructive evaluation of solid structural components) if fewer channels can be successfully utilized. The decrease in the number of TRM elements can be compensated by recording longer forward propagation signals at the TRM including multiple reflections from the boundaries and multiple scattering in presence of heterogeneities. Indeed, it has been shown that in the

<sup>a)</sup>Author to whom correspondence should be addressed. Electronic mail: tju@lanl.gov.

<sup>b)</sup>Electronic mail: mgriffa@lanl.gov.

latter case, the resulting outcome is equivalent to having a TRM with a higher effective aperture as if it was composed by more elements.<sup>27-31</sup>

However, the identification in space and time of a TR focal event with such a TRM can be problematic, especially in the case of focusing onto a scatterer location, which is initially unknown. Some imaging conditions based on sparsity norms have been proposed by Derveaux *et al.*<sup>32</sup> These conditions essentially rely on the fact that at the time of focus the backpropagated wave field is sharper and assumes higher values about and at the scatterer/source location. Sparsity norms, as the Shannon's entropy<sup>33</sup> or the bounded variation norm<sup>34</sup> of an image can help in identifying the right time of focus on a specific scatterer/source location.

In this paper, we propose a new and different imaging condition to aid in spatial focal event detection [imaging of the source(s)/scatterer(s)]. The corresponding metric function exploits the inherently symmetric nature of the TRP to find focal events in space at locations where the degree of temporal symmetry should be very high relative to a randomly selected spatial location. This paper will introduce the symmetry metric, provide experimental results, and give an analytical basis for the benefits of the imaging condition based on the proposed metric.

## II. EXPERIMENTAL DETAILS

The experimental results shown herein are all from the use of virtual pointlike sources. Virtual pointlike sources are created by measuring the direct elastic response  $R_B(t)$  at a selected position  $\mathcal{B}$  due to the input of an elastic pulse  $S_A(t)$  at the source transducer (position  $\mathcal{A}$ ). The response is measured with a laser vibrometer (spot size  $\sim 100 \mu\text{m}$ , velocity calibration of  $5 \text{ mm/s/V}$ ), which detects the out-of-plane particle vibration velocity wavefield on the surface of the specimen. Obviously, the laser cannot inject the TR response  $R_B(-t)$ . Instead,  $R_B(-t)$  is injected at the original source transducer at position  $\mathcal{A}$ . As a result of spatial reciprocity,<sup>35,36</sup>  $R_B(-t)$  refocuses at the original point of detection  $\mathcal{B}$  (i.e., the laser vibrometer). This method has been used for other experimental time reversal studies<sup>21,25,31,37</sup> and is a proven method for creating virtual sources without contacting the sample at the desired location of the virtual source.

Another advantage of this virtual source method is the ability to repeat the process for a second location  $\mathcal{B}'$  using the same source transducer at position  $\mathcal{A}$ . The sum of the two responses  $R_B$  and  $R_{B'}$  corresponds, in a linear elastic medium, to the signal recorded at location  $\mathcal{A}$  as if two sources were present at locations  $\mathcal{B}$  and  $\mathcal{B}'$ . Then, a complex virtual source can be created. Normalizing  $R_B$  and  $R_{B'}$  to different values before adding also allows one to vary the relative strengths of the multiple sources. Finally, positions  $\mathcal{B}$  and  $\mathcal{B}'$  can be located much closer than two finite size transducers, thus overlapping sources can be created for studying the resolution power of TRMs in localizing complex clusters of sources/scatterers. The latter type of investigation is of extreme importance for the nondestructive evaluation of microstructured and/or microdamaged materials.

In this study, we use a simple virtual source (i.e., only one position  $\mathcal{B}$ ) and later add to that a second virtual source at  $\mathcal{B}'$  such that the separation between the sources is  $\Delta r \leq \lambda_0/2$ , where  $\lambda_0$  is the wavelength corresponding to the dominant (i.e., central) frequency in the frequency band present in the source signal.  $\lambda_0/2$  corresponds to the resolution limit in the localization of the pointlike source using whatever imaging method, according to the Rayleigh criterion (see Ref. 2 and Refs. 9-12 therein).

After the virtual sources are created and signals are recorded and TR, the laser vibrometer is scanned around the area of the virtual source ( $20 \times 25 \text{ mm}^2$ ,  $0.5 \text{ mm}$  step size) during the backward propagation (rebroadcasting of TR signal from the original transducer). The resultant focused signals  $F_{\mathcal{N}}(t)$  are then recorded at each of the  $\mathcal{N}$  locations in the scan during the broadcast of  $R_B(-t)$ . In reality, the only signals that can be referred to as focused are those where  $\mathcal{N} = \mathcal{B}$ , or  $\mathcal{N} = \mathcal{B}'$  for multiple sources, and the immediate surrounding area defined by the diffraction limit, however, we refer to all signals  $F_{\mathcal{N}}$  as focused signals to refer to the fact that they are being recorded during the rebroadcast of  $R_B(-t)$  and have the potential to contribute to the focal event. From the collection of  $F_{\mathcal{N}}(t)$  at different scanning locations  $\mathcal{N}$ , it is then possible to create a spatial image at different times and discern the focal point using different methods. For example, the standard maximum-in-time amplitude-based imaging condition requires one to calculate the maximum amplitude in time of each signal  $F_{\mathcal{N}}(t)$ , for each scanning point  $\mathcal{N}$ , then to build the image using these maximum values. The backpropagated wave field assumes maximum values at source(s)/scatterer(s) location(s). To the contrary, imaging using sparsity norms consists in calculating at each time the value of the sparsity norm (Shannon's entropy of the image or its bounded variation norm), then selecting the image at the time when the norm assumes the global minimum value. Both imaging methods rely on the spatial focusing properties of the TR backpropagated fields. They coalesce at the location(s) of the original source(s)/scatterer(s), while they almost assume low values at other locations, at the time of focus. The new imaging method we propose herein is based on a different metric function, the symmetry metric function.

The sample used for all the experiments is a glass block measuring  $89 \times 89 \times 101 \text{ mm}^3$ , having a shear wave speed  $v_s = 2840 \text{ m/s}$ , and a quality factor  $Q = 1500$ . The original source transducer is a lead zirconate titanate-5 ceramic disk (diameter  $d = 38 \text{ mm}$ , thickness  $h = 2.8 \text{ mm}$ ) bonded to the sample using Devcon 2-ton epoxy. All virtual sources are created on a face orthogonal to that with the source transducer. Using only one source transducer equates to performing only single channel time reversal experiments (i.e., a single TRM element).<sup>30,31,37,38</sup> The initial source  $S_A$  used in all experiments is a  $10 \mu\text{s}$  sinusoid of frequency  $200 \text{ kHz}$  ( $\lambda_0 = 14.2 \text{ mm}$ ), shaped by a  $\sin^2$  envelope. This source function is emitted using a 12-bit D/A converter card (conversion rate of  $10 \text{ MHz}$ ) and the resulting responses recorded with a 14-bit A/D scope card sampling at  $1 \times 10^7$  samples/s.

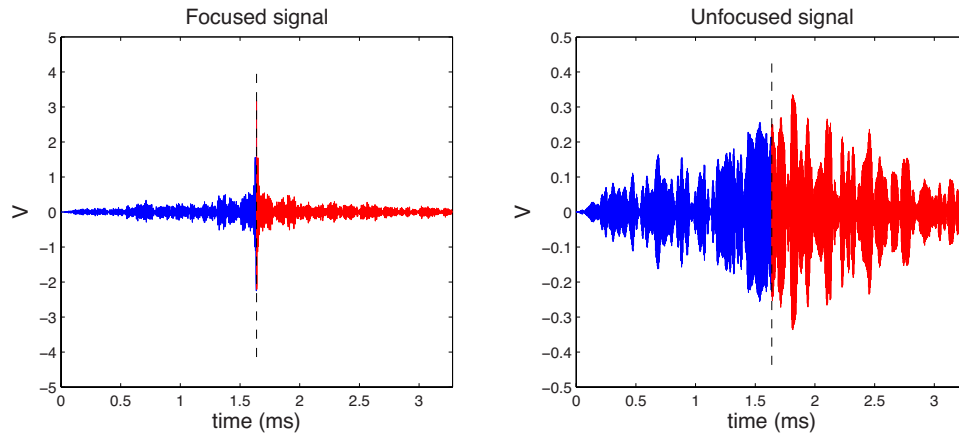


FIG. 1. (Color online) Two signals recorded at different spatial locations during the rebroadcast of the TR signal from a single channel. Left: signal located at the position of the original virtual source pulse. Right: signal recorded at an arbitrary position  $\sim 1$  cm away from the original virtual source. For the calculation of  $\Sigma_{\mathcal{N}}$  [Eq. (4)], each waveform is split at the time of focus  $t_F$  (here  $t_F = 1.6384$  ms, denoted by the vertical black dashed line and the change in color of the waveform from blue to red). The blue portion of the waveform illustrates  ${}^<F_{\mathcal{N}}$  while the red portion represents  ${}^>F_{\mathcal{N}}$ . Figure 2 shows the same two signals expanded around the focal time  $t_F$ .

### III. SYMMETRY METRIC-BASED IMAGING CONDITION

The symmetry metric  $\Sigma$  is essentially a zero-lag cross correlation-in-time between the incoming (collapsing) part and the outgoing part (source rebroadcast) of the TR back-propagated wave field, with the correlation operator ( $\otimes$ ) defined in the following manner,

$$(f \otimes g)(t) = \sum_{\tau} f^*(\tau)g(t + \tau), \quad (1)$$

where  $f(t)$  and  $g(t)$  are two time series (for example, wavefields evaluated at a spatial location), the discrete sum is used instead of an integral due to the fact that the signals being correlated are digitally sampled waveforms, not continuous functions, and  $*$  means the complex conjugate. As all waveforms are real, the complex conjugate ( $*$ ) of  $f(t)$  can be ignored in Eq. (1) for defining the zero-lag cross correlation.

At the time of focus, the wave collapses and the subsequent rebroadcast process should be an entirely symmetric event, as illustrated by the TRP being a realization of a matched filtering process, i.e., a temporal correlator (see Sec. I). It is possible to separate the focal signals into times before focusing (i.e., wavefront collapse,  $0 \leq t' \leq t_F$ ) and times after

focusing (i.e., source rebroadcast,  $t_F \leq t' \leq 2t_F$ ), where  $t_F$  is the focal time. Doing so allows for each  $F_{\mathcal{N}}(t')$  to be written as

$$F_{\mathcal{N}}(t') = \begin{cases} {}^<F_{\mathcal{N}}(t') & \text{for } 0 \leq t' \leq t_F \\ {}^>F_{\mathcal{N}}(t') & \text{for } t_F \leq t' \leq 2t_F. \end{cases} \quad (2)$$

It is necessary to note that  $t'$  here refers to the reversed time frame and is measured from the beginning of the backward propagation, i.e., running time backwards ( $t' = 2t_F - t$ ). Also note that the two halves of the focal signal are equal in duration. While it is not strictly necessary that all time from  $t = 0$  to  $t = 2t_F$  be measured, the symmetry calculation does require that the durations of  ${}^<F_{\mathcal{N}}(t')$  and  ${}^>F_{\mathcal{N}}(t')$  be equal.

To quantify this temporal symmetry, we simply split the focused signals  $F_{\mathcal{N}}$  at the appropriate focal time  $t_F$  as denoted above.  $t_F$  can be known *a priori* in the case of focusing at active source(s) location(s) or determined using some other method, for example using sparsity norms.<sup>32</sup> Once  $t_F$  is known and the signals separated into left and right hand sides, ( ${}^<F_{\mathcal{N}}$  and  ${}^>F_{\mathcal{N}}$ , respectively), as shown in Figs. 1 and 2, the two halves of the signals are vector normalized, e.g.,

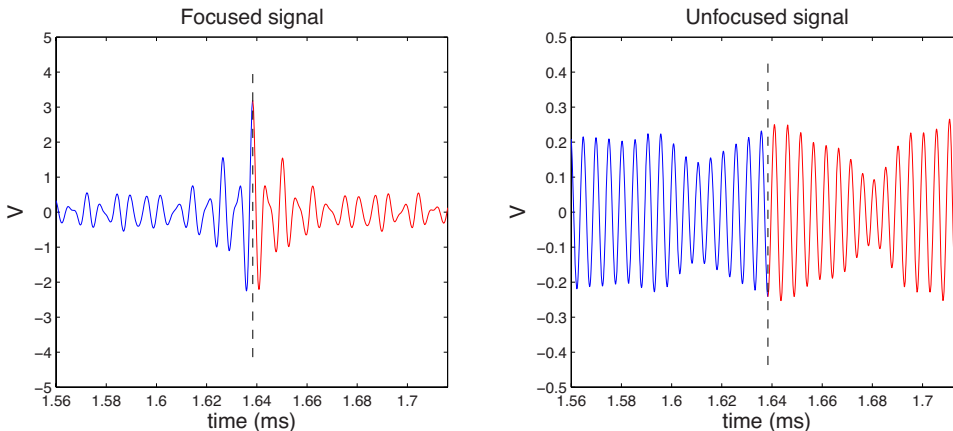


FIG. 2. (Color online) Same signals presented in Fig. 1. The  $x$ -axis has been expanded around the focal time,  $t_F = 1.6384$  ms, to show the fine structure of the waveforms.

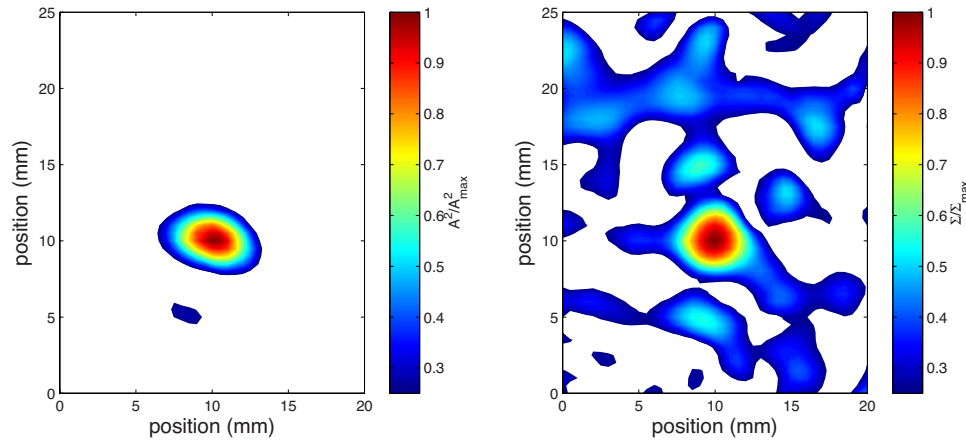


FIG. 3. (Color online) Spatial focusing image resulting from the TRP. Left: maximum-in-time amplitude squared ( $A^2$ ), right: symmetry ( $\Sigma$ ). Both images are normalized to the maximum values and the colormap floor is restricted to 0.25, to easily extract the resolution. Note the unfortunate additional noise introduced in the symmetry image; though this spatial noise does not inhibit the ability of the symmetry metric to more accurately reconstructs the original source shape. For the single pointlike source scenario, the symmetry of the focused signal adds little information, however, the added value of the symmetry measurement is apparent for more complex, or multiple sources (see Figs. 4 and 5).

$$\langle \tilde{F}_{\mathcal{N}} \rangle = \frac{\langle F_{\mathcal{N}} \rangle}{|\langle F_{\mathcal{N}} \rangle|}, \quad (3)$$

where  $|\langle F_{\mathcal{N}} \rangle|$  is the square root of the sum of the square of each value in time of the signal and the symbol  $\langle \tilde{F}_{\mathcal{N}} \rangle$  indicates the vector normalized version of the signal  $\langle F_{\mathcal{N}} \rangle$ . The right hand side is then TR  $[\langle \tilde{F}_{\mathcal{N}}(t') \rangle \rightarrow \langle \tilde{F}_{\mathcal{N}}(-t') \rangle]$  so that  $\Sigma_{\mathcal{N}}$ , the value of the symmetry metric function at the location  $\mathcal{N}$  in the sample, can be found from the zero-lag cross correlation,

$$\Sigma_{\mathcal{N}} = [\langle \tilde{F}_{\mathcal{N}}(t') \rangle \otimes \langle \tilde{F}_{\mathcal{N}}(-t') \rangle]_{t=0}. \quad (4)$$

In principle, as suggested above, a zero-lag cross correlation could be performed if  $t_F$  is known precisely. In practice, however, it is more prudent to calculate the cross-correlation function and then simply select the time when it achieves its maximum value. This allows for the precise timing of  $t_F$  to be unknown, however, to diminish “noise” in the  $\Sigma$  image, it is best to choose  $t_F$  as precisely as possible and restrict the selection of the maximum to within a short time interval about the zero-lag correlation time  $t=0$ . All  $\Sigma$  values here are extracted from the maxima lying within  $\pm 100 \mu\text{s}$  of  $t'=t_F$  (time of focus).

## IV. RESULTS

### A. Single source

Before examining the case with complex/multiple source(s), we first compare the use of the  $\Sigma$  metric function to the standard maximum-in-time amplitude ( $A$ ) method. It should be noted that before doing so, it is necessary to square the values from the maximum amplitude method to appropriately compare the results from the two techniques. This is necessary for the same reason that one must square the amplitude results before comparing to the image resulting from the  $E$  ( $E$ ) metric function. Indeed, energy and  $\Sigma$  calculations involve an integration over time of the product of two signals having the same physical dimension (the signal multiplied by itself and the signal multiplied by itself shifted in time, re-

spectively). In the limit that the waveform is shortened to one sample,  $\Sigma \propto E = A^2$ .

Figure 3 displays the experimental results from imaging a single pointlike source located at position (10, 10) mm on one lateral face of the glass block, using both the maximum-in-time and the symmetry imaging conditions. The feature that is immediately apparent is the increase in structure away from the location of focus that exceeds the floor of 0.25. This could be due to a few different reasons, but the most sensible here is the signal-to-noise level of the signals measured by the laser vibrometer, which has been seen by the authors to influence the  $\Sigma$  images more strongly than either the maximum amplitude or narrow time interval energy methods. This added spatial noise, however, does not prevent the position of the source to be located from the  $\Sigma$  image. In fact, the shape and extent of the original source is more accurately reproduced by the symmetry method, as the maximum amplitude metric produces a focus elongated in one dimension. Clearly, though, either method could stand alone to determine the focal position for a single source. It is interesting to note that the apparent spatial width at  $A^2/4$  is  $\sim 6$  mm, i.e.,  $\sim \lambda_0/2$ , indicating that we have reached or are very close to reaching the diffraction limit.

### B. Multiple sources

Multiple source detection using TRA is largely the same as that involving only a single source if the sources are well separated and the propagation medium is linear. The difficulty lies in the case when the sources become closely spaced, i.e.,  $\Delta r \leq \lambda_0/2$ . As the source separation  $\Delta r$  approaches this limit, the focal image resulting from employing a TRM shows only one focal point, as in Figs. 4 and 5. When  $\Delta r \approx \lambda_0/2$  the focal spot constructed from the maximum amplitude metric is elongated such that one might suspect the existence of multiple closely spaced sources or one source with an elongated dimension (Fig. 4). However, when  $\Delta r < \lambda_0/2$  the spatial extent of the focus constructed from  $A^2$  (Fig. 5) is no different than that for a single source (Fig. 3).

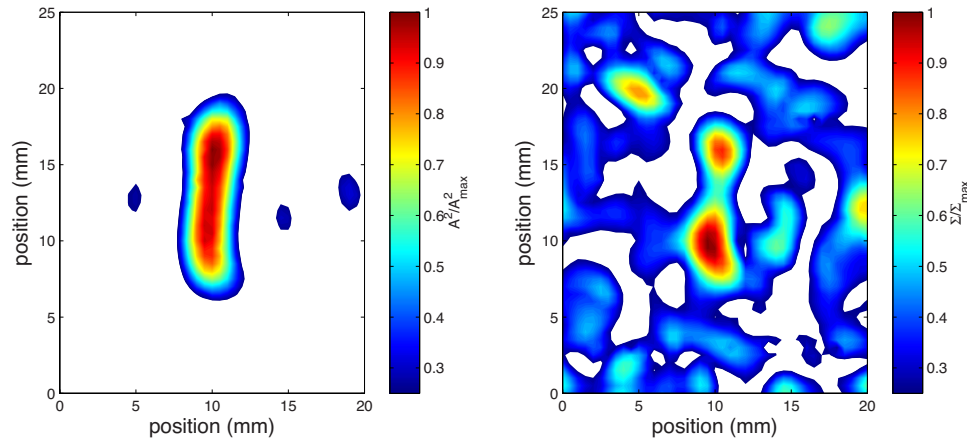


FIG. 4. (Color online) Spatial focusing image resulting from the TRP for two closely spaced sources (distance between the centers  $\Delta r = 6 \text{ mm} \approx \lambda_0/2$ ). Left: maximum-in-time amplitude squared ( $A^2$ ), right: symmetry ( $\Sigma$ ). Both images are normalized to the maximum values and the colormap floor is restricted to 0.25, to easily extract the resolution. Note the ability of the symmetry measurement to discern the two sources while the amplitude metric illuminates only one oblong source.

The  $\Sigma$  images for  $\Delta r \leq \lambda_0/2$ , in contrast to the  $A^2$  images, provide more details of the true extent of the source(s). For  $\Delta r \approx \lambda_0/2$ , the two sources are quite clearly separated. In the case of  $\Delta r < \lambda_0/2$ , while the two individual sources are not entirely separable, their extent is more accurately represented than what is shown in the  $A^2$  image, which is indistinguishable, apart from orientation, from the result for a single source.

## V. THEORETICAL ANALYSIS

As the  $\Sigma$  images are created from a different processing technique of the same data from which the  $A^2$  images are constructed, one might ask why the apparent increased resolution is manifest in the  $\Sigma$  images. The simple explanation is in the amount of data used to create the individual images. Creating an  $A$  (or  $A^2$ ) image is done by extracting the value of one sample in time from each waveform (i.e., the maximum) while the  $\Sigma$  image is created by extracting a single value (i.e., a correlation coefficient) by processing all of the

samples in each waveform. Thus the  $\Sigma$  metric is a more complete metric function resulting from the total amount of data available.

In the focal region as defined by the diffraction limit (i.e.,  $\rho \leq \lambda_0/2$ ,  $\rho \equiv$  distance from the center of focus) the symmetry measure is equivalent to measuring the spatial variation in the Green functions, as is illustrated in Figs. 6 and 7. This can be shown to be true analytically through the use of Green functions in describing single channel TRP. To do so we need only to make a few assumptions:

1. spatial reciprocity holds  $\rightarrow G(\mathcal{B}, t | \mathcal{A}, 0) = G(\mathcal{A}, t | \mathcal{B}, 0)$ , where  $G(\mathcal{Y}, t | \mathcal{X}, 0)$  indicates the Green function of the propagation medium evaluated at the location  $\mathcal{Y}$  at time  $t$  for a source at location  $\mathcal{X}$  starting at time 0;
2. temporally symmetric (or antisymmetric) source function  $\rightarrow S_{\mathcal{A}}(t) = S_{\mathcal{A}}(-t)$  or  $S_{\mathcal{A}}(t) = -S_{\mathcal{A}}(-t)$ ;
3. perfect source reproduction, i.e., the focused signal is the TR version of the source function  $\rightarrow F_{\mathcal{A}}(t) = S_{\mathcal{A}}(-t)$ .

The process then involves exploiting properties of tem-

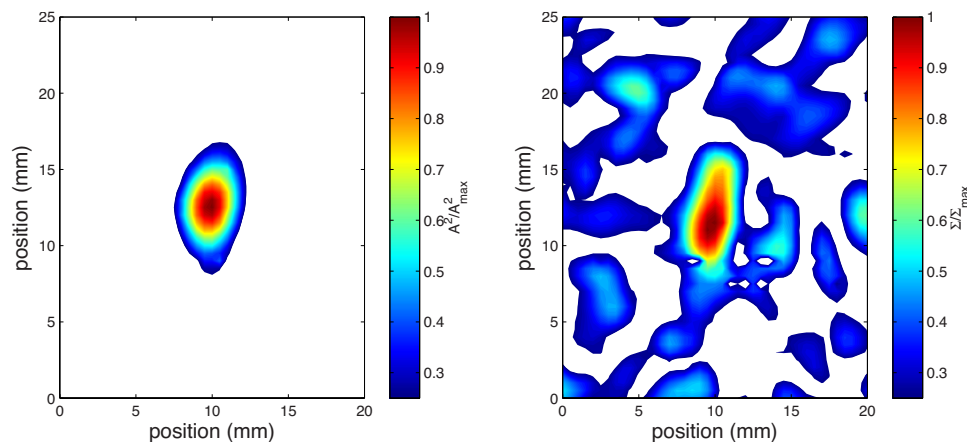


FIG. 5. (Color online) Spatial focusing image resulting from the TRP for two closely spaced sources (distance between the centers  $\Delta r = 5 \text{ mm} < \lambda_0/2$ ). Left: maximum-in-time amplitude squared ( $A^2$ ), right: symmetry ( $\Sigma$ ). Both images are normalized to the maximum values and the colormap floor is restricted to 0.25, to easily extract the resolution. Here the symmetry metric is not able to resolve the two sources completely, however, it does indicate an oblong source shape, as opposed to the circular source shape shown for a single source in Fig. 3. In both Figs. 3 and 5, the amplitude metric alone does not allow this same level of source shape/extent discrimination.

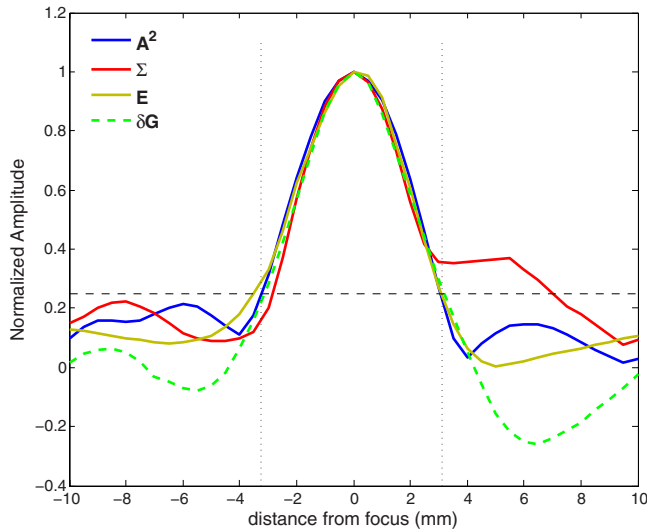


FIG. 6. (Color online) Spatial focusing comparison of maximum-in-time amplitude squared ( $A^2$ , solid blue line), the symmetry measure ( $\Sigma$ , solid red line), the energy metric ( $E$ , dark yellow line) and the spatial variation in the Green function ( $\delta G$ , dashed green line). The variation in the Green function is calculated by the Green function from the source transducer to the virtual source location ( $G_{AB}$ ) cross-correlated with the Green function from the same source location to each scanning position ( $G_{AN}$ ) with zero-lag (or shift) in the correlation. Note that all metrics define approximately the same focal extent for a single source, as indicated by the vertical black dotted lines.

poral convolutions, cross correlations and Green functions. To do this, it is necessary to define the notation to be used and can be seen in the description of the received signal  $R_B$  at point  $B$  due to a source at  $A$ ,

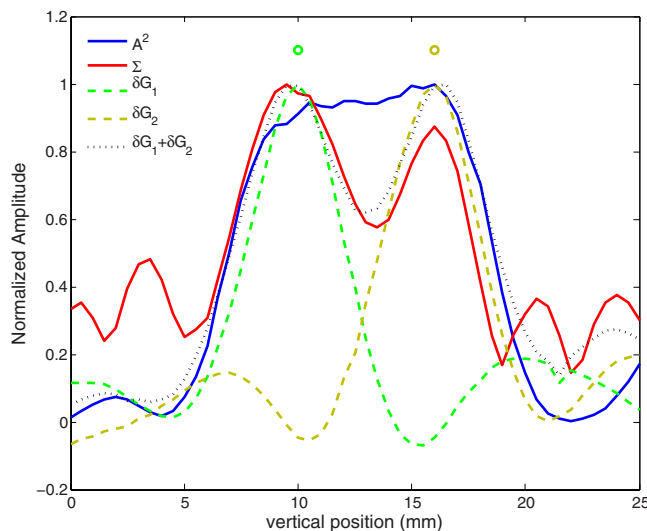


FIG. 7. (Color online) Spatial time reversal focusing in the case of two close-by point-like sources. Comparison between the maximum-in-time squared amplitude image ( $A^2$ , solid blue line) and the temporal symmetry image ( $\Sigma$ , solid red line). The images are calculated along the vertical line at  $X=10$  mm in the plane where both sources lay (see Fig. 4). The variation of the Green functions ( $\delta G_j$ ,  $j=1$  or  $2$ , respectively) as well as the linear superposition of these variations (i.e.,  $\delta G_1 + \delta G_2$ ) shown in the black dotted line. Additionally the original source locations are indicated by the two open circles at 10 and 16 mm.

$$R_B(t) = \sum_{\tau'} G(B, \tau' | A, 0) S_A(t - \tau'), \quad (5)$$

where the discrete sum is used instead of an integral again considering digitalized signals. The convolution operation above will be denoted in a simplified form for convenience. In this simplified notation, Eq. (5) becomes

$$R_B(t) = (G_{AB} \star S_A)(t), \quad (6)$$

where  $G_{AB}$  indicates the Green function from location  $A$  to location  $B$ . All waveforms are functions of time, as such this remains implied. The time frame of reference could be the normal (forward propagation) time frame or the TR frame resulting from the inversion-of-time operation  $t \rightarrow -t$ . In the latter case, a signal is denoted with a superscript “ $-$ ,” as in

$$R_B^-(t) = R_B(-t). \quad (7)$$

With the notation sufficiently defined, we can now look closely at the process of calculating the symmetry metric  $\Sigma_{\mathcal{N}}$  both at the focal location and away from the focus, i.e.,  $\mathcal{N} = A$  and  $\mathcal{N} = C$ , respectively.

### A. Focused Signal $F_A$

If the focal time  $t_F$  is known precisely and the focused signals split exactly at this time, then the maximum of the cross correlation will occur at the zero-lag (or zero-shift) correlation time, i.e.,  $t=0$  [see Eq. (1)]. For  $F_A$  this exercise is trivial, but we show it here for completeness. First, Eq. (2) is rewritten as

$$F_A = \begin{cases} < F_A = G_{BA} \star [G_{AB} \star S_A]^> & \text{for } 0 \leq t' \leq t_F \\ > F_A = S_A & \text{for } t_F < t' \leq T, \end{cases} \quad (8)$$

where  $T$  is the end time of the TR backpropagation. The second line in Eq. (8) descends directly from the third hypothesis previously. Thus

$$< \tilde{F}_A \otimes > \tilde{F}_A = < \tilde{F}_A \star > \tilde{F}_A = (G_{BA} \star G_{AB} \star S_A \star S_A) < m > m, \quad (9)$$

with  $< m > m$  being normalization constants. Using Eq. (6) and the relationship between the correlation and convolution operations (written here as  $\otimes$  and  $\star$ , respectively), it is possible to rewrite Eq. (9) as

$$< \tilde{F}_A \otimes > \tilde{F}_A = (R_B \otimes R_B) < m > m, \quad (10)$$

which makes it obvious that  $\Sigma = 1$  for a true focused signal as

$$\Sigma_A = [(R_B \otimes R_B) < m > m]_{r=0} = 1, \quad (11)$$

due to the fact that a normalized autocorrelation [i.e.,  $(R_B \otimes R_B) < m > m$ ] assumes value 1 at zero-lag time. This is a quick and crude way to demonstrate the TRP being a temporal correlator.<sup>8,9</sup> To understand the importance of the Green function's spatial variation it is necessary to similarly analyze an unfocused signal at an arbitrary location  $C$ .

### B. Unfocused Signal $F_C$

Equation (10) simply reiterates the known fact that the TRP is a temporal correlator and realizes a specific type of

matched filter. It must now be shown that unfocused signals cannot also produce the same result. To do so, Eq. (2) must be written for some arbitrary location  $C$ .

$$F_C = \begin{cases} <F_C = G_{BC} \star [G_{AB} \star S_A]> & \text{for } 0 \leq t' \leq t_F \\ >F_C = G_{AC} \star S_A & \text{for } t_F < t' \leq T. \end{cases} \quad (12)$$

Performing the cross correlation for  $F_C$  using Eq. (12), we have

$$\begin{aligned} <\tilde{F}_C \otimes >\tilde{F}_C &= <\tilde{F}_C \star >\tilde{F}_C \\ &= (G_{BC} \star G_{AB} \star S_A^- \star G_{AC} \star S_A)^{<n>n} \\ &= (G_{BC} \star \mathcal{G}_{AB} \star \mathcal{G}_{AC})^{<n>n}, \end{aligned} \quad (13)$$

where the normalization constants are now  $<n$  and  $>n$ , and  $\mathcal{G}$  is the limited band Green function (or impulse response) defined by the bandwidth present in the source  $S_A$ . You can see that the source terms (i.e.,  $S_A^- \star S_A$ ) have been removed and the Green functions have been changed to represent the limited band.

This bandwidth limiting can be shown to be true by performing a cross correlation of the original received signal  $R_B$  from Eq. (5) and the source, as in

$$\mathcal{H}_{AB} \equiv R_B \otimes S_A. \quad (14)$$

Here  $\mathcal{H}_{AB}$  is the limited band impulse response, which we can show is proportional to our  $\mathcal{G}_{AB}$  by transforming into the frequency domain,

$$\mathcal{H}_{AB}(\omega) \equiv R_B(\omega) S_A^*(\omega) = G_{AB}(\omega) S_A(\omega) S_A^*(\omega). \quad (15)$$

It is apparent by looking at the frequency domain that  $\mathcal{H}_{AB}(\omega)$  will only have the frequency content of source  $S_A$ . It is true that only for a source with a constant bandwidth (e.g., a chirp), will  $\mathcal{H}_{AB} \propto G_{AB}$ , however, empirically we have seen during extensive experiments that for sources used in our experiments (i.e.,  $\sin^2$  enveloped sinusoids) for all practical purposes  $\mathcal{H}_{AB} \approx G_{AB}$ .

Getting back to the asymmetry of  $\Sigma_C$ , we can see that

$$\Sigma_C = [(G_{BC} \star \mathcal{G}_{AB} \star \mathcal{G}_{AC})^{<n>n}]_{t=0}. \quad (16)$$

The normalization restricts the values of  $|\Sigma_C|$  to be between 0 and 1, thus, we can obtain a value of 1 in the event that  $\mathcal{G}_{BC} = \mathcal{G}_{AB} = \mathcal{G}_{AC}$ , which is only possible in the uninteresting scenario  $A=B=C$ . Also in the limit that  $C \rightarrow A$ ,

$$\Sigma_C = [(G_{BA} \star \mathcal{G}_{AB} \otimes \text{const.})^{<n>n}]_{t=0} = \Sigma_A. \quad (17)$$

We can recover the solution for the true focused signal similar to that given in Eq. (11). It is also possible to show a similar result for the case of  $C \rightarrow B$ . Now it is apparent that, except for the three trivial cases of  $C \rightarrow A$ ,  $C \rightarrow B$ , and  $C = B = A$ , we should always have  $\Sigma_C < 1$ .

Close to the true focal point the change in  $\mathcal{G}_{AC}$  varying  $C$  is negligible, thus  $\mathcal{G}_{AC}$  can be taken as a constant. For this to be true, the separation of the two evaluation points,  $A$  and  $C$ , should be  $\Delta \leq \lambda_0/4$ , i.e., within the focal spot determined by the diffraction limit of the frequencies used. This limit on the separation distance  $\Delta$  is purely empirical, but is not unreasonable.

When  $\mathcal{G}_{AC}$  can be taken as a constant, then the calculation for  $\Sigma_C$  becomes

$$\Sigma_C = [(G_{BC} \star \mathcal{G}_{AB})^{<n>n}]_{t=0} = [(G_{BC} \star \mathcal{G}_{AB}^-)^{<n>n}]_{t=0}. \quad (18)$$

Experimentally one can verify this by recalling Eq. (14) and that  $\mathcal{G}_{AB} \approx \mathcal{H}_{AB}$ . Obtaining a set of  $\mathcal{G}_{NM}$ s at and near a true focal point, the calculation of the  $\Sigma_{MS}$ s from the set of focused signals (i.e.,  $F_{MS}$ s) can be compared to the spatial variation ( $\delta G$ ) in the Green functions from

$$\delta G = N[\mathcal{G}_{NM_0} \otimes \mathcal{G}_{NM_0+\delta M}]_{t=0}. \quad (19)$$

Here  $M_0 \equiv$  focal point and  $N$  is yet another normalization constant. The results of conducting this comparison for a single source can be found in Fig. 6. For multiple sources in a linear medium, the same comparison can be made, however, now a  $\delta \mathcal{G}_j$  must be found for each source  $j$  and the results added linearly (if all sources are present simultaneously) before comparing to the symmetry measure. Figure 7 displays the results of the comparison for two simultaneous identical sources separated by a distance  $d = \lambda_0/2$ .

Also included in Fig. 7 is what we refer to as the energy metric. This quantity is simply the energy (in arbitrary units) in the focus interval  $2\Delta\tau$  as calculated by

$$E_N = \sum_{\tau=t_F-\Delta\tau}^{t_F+\Delta\tau} S_N^2(\tau). \quad (20)$$

## VI. DISCUSSION

This paper introduces a new imaging condition, based on the temporal symmetry metric function  $\Sigma$  to aid in spatial localization and characterization of TR foci. It essentially exploits the basic feature of TR backpropagated wavefields to be symmetric in time about the time of focus mainly at the spatial focal location and not elsewhere. An analytical explanation and experimental tests results are given to show  $\Sigma$  to be a complementary tool for locating focal locations and in characterizing their complexity.  $\Sigma$  takes advantage of a larger set of temporal data than an maximum-in-time amplitude squared ( $A^2$ ) display, and is therefore better able to distinguish source complexity.  $\Sigma$  is prone to a higher noise floor than  $A^2$  but a combination of the two metrics ( $\Sigma * A^2$ ) is better than either one alone. The  $\Sigma$  imaging method can also better help in the simultaneous localization of multiple sources/scatterers. Indeed, other time reversal imaging conditions, as the ones based on sparsity norms,<sup>32</sup> can only produce distinct images highlighting the focusing on single distinct sources/scatterers. Then, the set of images need to be added, with the side effect of adding also noise patterns and ghost images of foci.

## ACKNOWLEDGMENTS

The work was supported by Institutional Support (LDRD) at the Los Alamos National Laboratory. The authors are grateful for invaluable input from Robert Guyer, Paul Johnson, and Carene Larmat.

<sup>1</sup>M. Fink, *IEEE Trans. Ultrason. Ferroelectr. Freq. Control* **39**, 555 (1992).

<sup>2</sup>D. Cassereau and M. Fink, *IEEE Trans. Ultrason. Ferroelectr. Freq. Con-*



- rol **39**, 579 (1992).
- <sup>3</sup>M. Fink, D. Cassereau, A. Derode, C. Prada, P. Roux, M. Tanter, J. L. Thomas, and F. Wu, *Rep. Prog. Phys.* **63**, 1933 (2000).
- <sup>4</sup>F. Wu, J. L. Thomas, and M. Fink, *IEEE Trans. Ultrason. Ferroelectr. Freq. Control* **39**, 567 (1992).
- <sup>5</sup>M. Fink and C. Prada, *Inverse Probl. Eng.* **17**, R1 (2001).
- <sup>6</sup>M. Fink, *Sci. Am.* **281**, 91 (1999).
- <sup>7</sup>B. E. Anderson, M. Griffa, C. Larmat, T. J. Ulrich, and P. A. Johnson, *Acoustics Today* **4**, 5 (2008).
- <sup>8</sup>M. Tanter, J.-L. Thomas, and M. Fink, *J. Acoust. Soc. Am.* **108**, 223 (2000).
- <sup>9</sup>C. Dorme and M. Fink, *J. Acoust. Soc. Am.* **98**, 1155 (1995).
- <sup>10</sup>M. Fink, *Phys. Scr., T* **90**, 268 (2001).
- <sup>11</sup>I. Tolstoy and C. Clay, *Ocean Acoustics. Theory and Experiment in Underwater Sound* (McGraw-Hill, New York, 1966), Chap. 7, pp. 243–268.
- <sup>12</sup>W. A. Kupermann and D. R. Jackson, *Imaging of Complex Media with Acoustic and Seismic Waves* (Springer-Verlag, Berlin, 2002), Vol. 84, pp. 93–97.
- <sup>13</sup>C. Prada, M. Fink, and F. Wu, *J. Acoust. Soc. Am.* **90**, 1119 (1991).
- <sup>14</sup>C. Prada and M. Fink, *Wave Motion* **20**, 151 (1994).
- <sup>15</sup>C. Prada, S. Manneville, D. Spoliansky, and M. Fink, *J. Acoust. Soc. Am.* **99**, 2067 (1996).
- <sup>16</sup>G. Montaldo, M. Tanter, and M. Fink, *J. Acoust. Soc. Am.* **512**, 776 (2004).
- <sup>17</sup>B. E. Anderson, M. Scalerandi, A. S. Gliozzi, M. Griffa, T. J. Ulrich, and P. A. Johnson, *Review of Progress in Quantitative Nondestructive Evaluation*, edited by D. O. Thompson and D. E. Chimenti (American Institute of Physics, New York, 2008), Vol. 27B, pp. 1520–1527.
- <sup>18</sup>S. K. Lehman and A. J. Devaney, *J. Acoust. Soc. Am.* **113**, 2742 (2003).
- <sup>19</sup>F. K. Gruber, E. A. Marengo, and A. J. Devaney, *J. Acoust. Soc. Am.* **115**, 3042 (2004).
- <sup>20</sup>E. A. Marengo, F. K. Gruber, and F. Simonetti, *IEEE Trans. Image Process.* **16**, 1967 (2008).
- <sup>21</sup>T. J. Ulrich, P. A. Johnson, and A. Sutin, *J. Acoust. Soc. Am.* **119**, 1514 (2006).
- <sup>22</sup>A. S. Gliozzi, M. Griffa, and M. Scalerandi, *J. Acoust. Soc. Am.* **120**, 2506 (2006).
- <sup>23</sup>T. J. Ulrich, P. A. Johnson, and R. A. Guyer, *Phys. Rev. Lett.* **98**, 104301 (2007).
- <sup>24</sup>T. Goursolle, S. Calle, S. Dos Santos, and O. Bou Matar, *J. Acoust. Soc. Am.* **122**, 3220 (2007).
- <sup>25</sup>J. de Rosny and M. Fink, *Phys. Rev. Lett.* **89**, 124301 (2002).
- <sup>26</sup>M. Griffa, B. E. Anderson, R. A. Guyer, T. J. Ulrich, and P. A. Johnson, *J. Phys. D: Appl. Phys.* **41**, 085415 (2008).
- <sup>27</sup>A. Derode, P. Roux, and M. Fink, *Phys. Rev. Lett.* **75**, 4206 (1995).
- <sup>28</sup>P. Roux, B. Roman, and M. Fink, *Appl. Phys. Lett.* **70**, 1811 (1997).
- <sup>29</sup>P. Roux and M. Fink, *J. Acoust. Soc. Am.* **107**, 2418 (2000).
- <sup>30</sup>C. Draeger and M. Fink, *J. Acoust. Soc. Am.* **105**, 611 (1999).
- <sup>31</sup>C. Draeger and M. Fink, *J. Acoust. Soc. Am.* **105**, 618 (1999).
- <sup>32</sup>G. Derveaux, G. Papanicolaou, and C. Tsokga, *J. Acoust. Soc. Am.* **121**, 2071 (2007).
- <sup>33</sup>C. E. Shannon, *Bell Syst. Tech. J.* **27**, 379 (1948).
- <sup>34</sup>T. F. Chan and J. Shen, *Image Processing and Analysis* (Society for Industrial and Applied Mathematics, Philadelphia, 2005).
- <sup>35</sup>J. M. Carcione, *Wave Fields in Real Media: Wave propagation in Anisotropic, Anelastic, Porous and Electromagnetic Media* (Elsevier, New York, 2007), Vol. 38.
- <sup>36</sup>J. D. Achenback, *Reciprocity in Elastodynamics* (Cambridge University Press, Cambridge, 2003).
- <sup>37</sup>A. Sutin, J. A. TenCate, and P. A. Johnson, *J. Acoust. Soc. Am.* **116**, 2779 (2004).
- <sup>38</sup>C. Draeger and M. Fink, *Phys. Rev. Lett.* **79**, 407 (1997).